JOURNAL OF AIRCRAFT
Vol. 42, No. 6, November–December 2005

Aircraft Spin Recovery, with and without Thrust Vectoring, Using Nonlinear Dynamic Inversion

P. K. Raghavendra,* Tuhin Sahai,* P. Ashwani Kumar,† Manan Chauhan,‡ and N. Ananthkrishnan§
Indian Institute of Technology Bombay, Mumbai 400 076, India

The present paper addresses the problem of spin recovery of an aircraft as a nonlinear inverse dynamics problem of determining the control inputs that need to be applied to transfer the aircraft from a spin state to a level trim flight condition. A stable, oscillatory, flat, left spin state is first identified from a standard bifurcation analysis of the aircraft model considered, and this is chosen as the starting point for all recovery attempts. Three different symmetric, level-flight trim states, representative of high, moderate, and low-angle-of-attack trims for the chosen aircraft model, are computed by using an extended-bifurcation-analysis procedure. A standard form of the nonlinear dynamic inversion algorithm is implemented to recover the aircraft from the oscillatory spin state to each of the selected level trims. The required control inputs in each case, obtained by solving the inverse problem, are compared against each other and with the standard recovery procedure for a modern, low-aspect-ratio, fuselage heavy configuration. The spin recovery procedure is seen to be restricted because of limitations in control surface deflections and rates and because of loss of control effectiveness at high angles of attack. In particular, these restrictions adversely affect attempts at recovery directly from high-angle-of-attack oscillatory spins to low-angle-of-attack trims using only aerodynamic controls. Further, two different control strategies are examined in an effort to overcome difficulties in spin recovery because of these restrictions. The first strategy uses an indirect, two-step recovery procedure in which the airplane is first recovered to a high- or moderate-angle-of-attack level-flight trim condition, followed by a second step where the airplane is then transitioned to the desired low-angle-of-attack trim. The second strategy involves the use of thrust-vectoring controls in addition to the standard aerodynamic control surfaces to directly recover the aircraft from high-angle-of-attack oscillatory spin to a low-angle-of-attack level-flight trim state. Our studies reveal that both strategies are successful, highlighting the importance of effective thrust management in conjunction with suitable use of all of the aerodynamic control surfaces for spin recovery strategies.

I. Introduction

SPIN has been and continues to be one of the most complex and dangerous phenomena encountered in flight. Stall/spin-related incidents account for a significant proportion of accidents in both military and general aviation airplanes.[1,2] Not surprisingly, spin prediction and spin recovery have been issues that have attracted considerable attention among flight dynamicists over the years.[3] By the early 1980s, approximate methods based on reduced-order models had been developed for equilibrium spin prediction.[4,5] (For definitions of various spin types or modes—equilibrium or steady vs oscillatory, erect vs inverted, flat vs steep, etc.—the reader is referred to standard books, e.g., Ref. 6.) The introduction of bifurcation methods around that period, however, brought about a major advancement in spin prediction capabilities.[7,8] It became possible to work with the complete equations of aircraft motion with no approximation and to numerically compute not just equilibrium spin states but also oscillatory spin solutions.[9,10] Jumps from a nonspin state to a spin state, or between two different spin states, hysteresis, and other nonlinear phenomena observed in poststall flight could also be predicted.[11,12] One could even think in terms of a spin prevention/recovery control system based on the results of a bifurcation analysis for a given aircraft.[13]

One strategy for spin prevention is to avoid the jump phenomenon leading to spin entry by suitably scheduling the control surfaces in either a feedforward or a feedback manner.[7,14] Control scheduling effectively changes the topology of the equilibrium spin solutions at high angles of attack, either eliminating the stable spin solutions or deleting the bifurcation points at which departure to spin occurs.[15] However, bifurcation analysis essentially presents a quasi-static picture of the aircraft dynamics, and consequently, control schedules deduced from the results of a bifurcation analysis are also quasi-static in nature. Such control strategies are not always successful in practice, and when they do succeed, the solutions typically turn out to be suboptimal.[7] Instead, a better approach would be to use the results from a bifurcation analysis as a guide to designing a nonlinear control law that can extend the stable flight envelope of the airplane by removing the bifurcation points that give rise to onset of spin.[16] However, given the possibility that a variety of complex aerodynamic phenomena might be encountered at high angles of attack, it has not been possible to come up with a simple, reliable, and foolproof control system that can, without seriously reducing aircraft maneuverability, guarantee protection against entry into spin.[13] Instead, attention has been focused on devising control systems for spin recovery.

Piloting strategies for spin recovery have undergone drastic changes over the years.[3] In the initial years, the prescription for spin recovery was to increase the thrust and simultaneously apply rudder to oppose the rotation. Later, as airplanes grew wing heavy, downelevator became the primary control input applied to recover from spin. For modern military aircraft, with low-aspect-ratio wings, which are fuselage heavy, the primary spin recovery control has been aileron with the spin, supplemented with rudder against the direction of rotation. However, present-generation military airplanes frequently exhibit oscillatory spins requiring nonstandard and nonintuitive control inputs for recovery. For example, steady and oscillatory spins for the F-14 were studied in Ref. 17, and attempts at spin recovery were made based on the results of the bifurcation analysis carried out to predict the various spin solutions. Unfortunately, none of the

Presented as Paper 2004-0378 at the AIAA Aerospace Sciences Meeting and Exhibit, Reno, NV, 5–8 January 2004; received 15 July 2004; revision received 6 October 2004; accepted for publication 9 October 2004.

*Masters (Dual Degree) Student.
†Undergraduate Student.
‡Research Assistant.
§Associate Professor, Department of Aerospace Engineering; akn@aero.iitb.ac.in. Senior Member AIAA.

control strategies tried out for spin recovery were successful, possibly because of the quasi-static nature of the bifurcation analysis results, as pointed out earlier. In particular, the tendency for a stable equilibrium spin, on application of recovery controls, to give way to a sustained oscillatory spin was observed. It was concluded that it was very important to account for oscillatory spin modes when considering spin recovery strategies.

Control strategies for aircraft spin recovery are necessarily complex and nonlinear.[18] Synthesis of a nonlinear controller for recovery of an unstable aircraft from a time-dependent spin mode was attempted in Ref. 19. Following a two-step procedure, they first stabilized the aircraft at a high-angle-of-attack equilibrium spin state and then applied a predefined set of control inputs to recover the aircraft to a low-angle-of-attack trim. Initial attempts, however, were met with failure, and extensive studies had to be carried out to generate a set of control inputs that could achieve recovery.

Properly speaking, the problem of spin recovery is one of determining the control inputs that need to be applied to transfer the aircraft from a spin state S to a level-trim-flight condition L. The control strategy for spin recovery therefore requires a solution of what is called the inverse problem of flight dynamics.[20] A solution to the inverse problem has been possible by use of the theory of nonlinear dynamic inversion applied to the equations of aircraft dynamics.[21] However, dynamic inversion in its basic, first-order form requires as many control inputs as state variables, which is generally not the case for aircraft flight dynamics. This problem was overcome by deriving dynamic inversion laws for flight control based on a decomposition of the aircraft dynamics into fast inner-loop dynamics for the angular rates and slow outer-loop dynamics for the attitude variables.[22,23] Dynamic inversion in this form has been applied to nonlinear flight maneuvers,[24] trajectory control,[25] poststall flight,[26] and for many other applications.[27] It is apparent that the method of nonlinear dynamic inversion is ideally suited for solving the problem of recovering an aircraft from spin to a level-trim-flight condition.

The present paper addresses the problem of spin recovery of an aircraft using nonlinear dynamic inversion techniques. In particular, we first consider the problem of determining the control inputs that need to be given to recover an airplane from an oscillatory spin state to three different level-flight conditions representing high-, moderate-, and low-angle-of-attack trim states, respectively. The aircraft model used for this study is the F-18/HARV, which has been used several times in the past as a testbed for research associated with high-angle-of-attack dynamics and control.[24,28–30] Both equilibrium and oscillatory spin states are identified by carrying out a standard bifurcation analysis (SBA) of the open-loop aircraft dynamics model. Computation of stable, level-flight-trim states to which the airplane could be recovered is done by using an extended-bifurcation-analysis (EBA) procedure, as proposed in Ref. 31. Three branches of stable, level-flight trims are identified from the EBA computations at high, moderate, and low values of angle of attack. One representative trim state, labeled A, B, and C, respectively, is selected from each of these stable, level-flight branches. The dynamic inversion algorithm in the form proposed in Ref. 26 is implemented to recover the aircraft from an oscillatory spin state to each of the level trims, A, B, C. The required control inputs in each case, obtained by solving the inverse problem, are compared against each other and with the standard recovery controls for a modern, low-aspect-ratio, fuselage heavy configuration.

It is well known, and is also observed in our studies, that the spin recovery procedure is restricted because of limitations in control surface deflections and rates and because of loss of control effectiveness at high angles of attack. In particular, these restrictions can adversely affect attempts at recovery directly from high-angle-of-attack oscillatory spins to low-angle-of-attack trims using only aerodynamic controls. In the second part of this paper, two different control strategies are examined in an effort to overcome difficulties in spin recovery as a result of these restrictions. The first strategy uses an indirect, two-step recovery procedure in which the airplane is first recovered to a high- or moderate-angle-of-attack level-flight trim condition, followed by a second step where the airplane is then transitioned to the desired low-angle-of-attack trim. The second strategy involves the use of thrust-vectoring controls in addition to the standard aerodynamic control surfaces to directly recover the aircraft from high-angle-of-attack oscillatory spin to a low-angle-of-attack level-flight trim state.

The potential of thrust vectoring as a tool for poststall maneuvering[32] and spin recovery[33] has been examined in the past, but with mixed results. In Ref. 33, using bifurcation methods, it was possible to deduce the direction in which the thrust-vectoring nozzles ought to be deflected in order to aid in spin recovery, but not the precise amount of deflection nor the moment at which the vectoring control was to be removed. Simulations showed that improper vectoring nozzle deflection angles or delayed removal of the thrust-vectoring controls could drive the airplane into deeper, oscillatory spin, or even push it into a spin with opposite rotation. Again employing bifurcation analysis as a tool, Ref. 34 showed that it was possible to use pitch thrust vectoring to eliminate an oscillatory spin state and replace it with a symmetric high-angle-of-attack trim. Unfortunately, in this process a new stable steep spin branch gets created, and simulations reveal that application of recovery controls from the oscillatory spin state leads to the aircraft dynamics being attracted to the newly formed steep spin solution. Poststall pitch reversal maneuvers have, however, been successfully simulated recently in Ref. 35 for the F-18/HARV airplane, including thrust-vectoring controls, using the nonlinear dynamic inversion control law presented in Ref. 26. Following the work in Ref. 35, our proposal to use a dynamic inversion algorithm to examine the effectiveness of thrust vectoring controls in spin recovery gains interest. Our studies reveal that both the strategies, the first involving a two-step angle-of-attack command along with an increase in static thrust to trim at an intermediate high/moderate-angle-of-attack level trim state and the second employing pitch and yaw thrust vectoring, are successful in spin recovery to a low-angle-of-attack level-flight trim condition. These results highlight the importance of effective thrust management in conjunction with suitable use of all of the aerodynamic control surfaces for successful spin recovery strategies.

II. Bifurcation Analysis for Spin Prediction

The aircraft dynamics equations used for this study have been presented in full in Appendix A. The complete system of equations can be represented as follows:

$$\dot{\boldsymbol{x}} = f(\boldsymbol{x}, \boldsymbol{u}) \tag{1}$$

where $\boldsymbol{x}$, the vector of state variables, and $\boldsymbol{u}$, the vector of control inputs, consist of the following elements:

$$\boldsymbol{x} = [V, \alpha, \beta, p, q, r, \phi, \theta, \psi, X, Y, Z]$$

$$\boldsymbol{u} = [\delta e, \eta, \delta a, \delta r, \delta pv, \delta yv]$$

In keeping with the standard practice, a subset of Eq. (1) consisting of the eight state equations in the first eight variables of the vector $\boldsymbol{x}$, as follows,

$$\dot{\boldsymbol{x}}_1 = f_1(\boldsymbol{x}_1, \boldsymbol{u}) \tag{2}$$

where

$$\boldsymbol{x}_1 = [V, \alpha, \beta, p, q, r, \phi, \theta]$$

is considered for the bifurcation analysis to determine the equilibrium states and limit cycles and their stability. All simulations of the aircraft dynamics are, however, carried out with the complete set of 12 equations in Eq. (1). The control deflections, their position and rate limits, and the various constants used in the simulations are defined and their values given in Appendix A (see Tables A1 and A2).

To identify the spin solutions for the aircraft model under consideration, the AUTO continuation and bifurcation algorithm[36] is used to carry out a SBA of the aircraft dynamics.[31] The AUTO code was enabled to handle stability/control derivative data in the tabular look-up format as specified in Table A3 in Appendix A. The data for each stability/control derivative were originally available

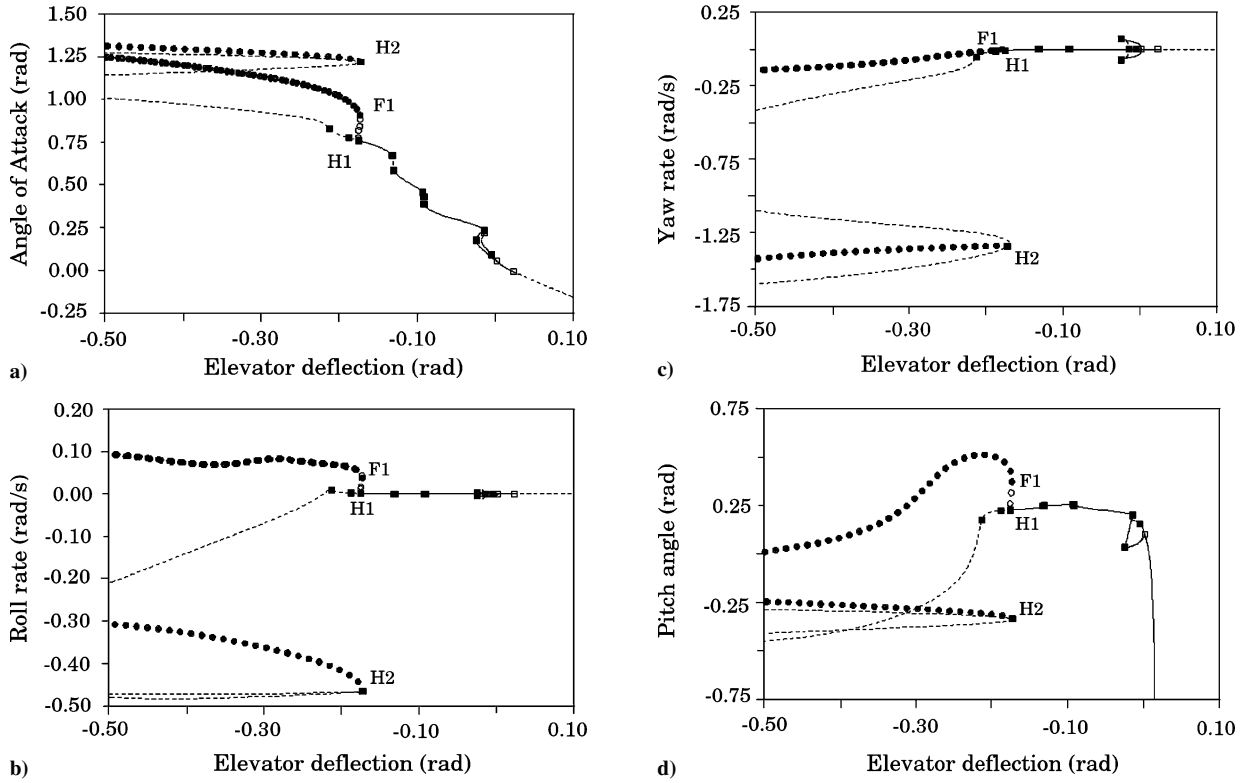

Fig. 1 Bifurcation diagram of a) angle of attack α, b) roll rate p, c) yaw rate r, and d) pitch angle θ, with elevator deflection δe as the continuation parameter: ——, stable equilibria; - - - -, unstable equilibria; ■■■, Hopf bifurcation points; □□□, pitchfork or transcritical bifurcation points; ● ● ●, peak amplitude of stable limit cycles; and ○ ○ ○, peak amplitude of unstable limit cycles.

at intervals of 4 deg in angle of attack. Each interval was further discretized into subintervals of 1 deg each, and AUTO was programmed to evaluate the aerodynamic coefficients by using a linear interpolation between the newly created 1-deg subintervals. This was found to greatly improve the smooth running of AUTO and nearly eliminated all instances of abnormal termination during the running of the code. Alternatively, a cubic-spline interpolation of the original data points at 4-deg intervals was provided to AUTO, and it was found that the solutions were identical to those obtained from the linear interpolation scheme described earlier. However, the cubic-spline interpolation significantly increased the run time, and it was therefore discarded in favor of the linear interpolation scheme.

The AUTO code requires an equilibrium state to be specified as a starting point for the continuation algorithm, which will then be used to compute all other equilibrium states along that solution branch. Any equilibrium state on a solution branch is equally acceptable as a starting point, as AUTO computes the entire branch of equilibrium solutions irrespective of the starting point. For convenience, a straight and level, symmetric flight trim is chosen as a starting point for the AUTO continuation algorithm, as follows:

$$[V, \alpha, \beta, p, q, r, \phi, \theta]$$

$$= [661 \text{ ft/s}, 0.035 \text{ rad}, 0, 0, 0, 0, 0, 0.035 \text{ rad}]$$

$$[\delta e, \eta, \delta a, \delta r, \delta pv, \delta yv] = [0.006 \text{ rad}, 0.38, 0, 0, 0, 0]$$

Elevator deflection δe is used as the continuation parameter for the SBA, with all of the other controls kept constant at the preceding values. Results from the SBA computation are shown in Figs. 1a–1d, and are discussed next.

Figure 1a shows the equilibrium values of angle of attack α as a function of elevator deflection δe. Over the low to moderate α range between 0 and 43 deg (0.75 rad), the aircraft dynamics consists mostly of stable equilibria with very short stretches of unstable equilibrium points bounded on either side by Hopf bifurcations (marked with filled squares). Figures 1b and 1c show, respectively, the roll rate and yaw rate for these equilibria to be zero; sideslip and roll angle (not shown in the figures) are also zero, thereby indicating that these equilibria correspond to symmetric flight. Equilibrium solutions for negative values of angle of attack are unstable as a result of the loss of spiral stability and are not of interest to the present study. At the other end of the stable branch of equilibria, beyond the Hopf bifurcation marked H1 at 43-deg angle of attack the equilibrium solutions are all unstable. Instead, a branch of unstable limit cycles is created at H1, which turns stable at a fold bifurcation marked F1 at $\alpha \approx 50$ deg (0.875 rad). The limit-cycle motion on this branch can be seen from Figs. 1b–1d to consist predominantly of a pitching oscillation, accompanied by comparatively smaller roll and yaw rates, which is sometimes called "bucking" or "pitch rocking."

Figures 1b and 1c reveal that the unstable equilibrium solutions beyond the Hopf bifurcation H1 deviate toward negative roll and yaw rates. This is caused by nonzero and asymmetric values of the lateral force and moment coefficients as a result of right and left elevator deflection at higher angles of attack.

Figure 1a further shows an apparently unconnected branch of unstable equilibrium solutions at high angles of attack between 65 deg (1.14 rad) and 72 deg (1.25 rad). These equilibria were obtained by continuing the computations beyond the up-elevator deflection limit to the left of Fig. 1a, where the branch of unstable solutions passing through H1 was seen to fold back and reappear in the figure as a high-angle-of-attack equilibrium branch. Figures 1b and 1c show these equilibria to correspond to an unstable equilibrium spin solution with high negative roll and yaw rates. A stable oscillatory spin solution is seen to emerge from this unstable equilibrium branch at a Hopf bifurcation point marked H2 at an angle of attack of about 70 deg (1.22 rad). The Mach number over this stable limit-cycle spin branch is observed to be in the range 0.16–0.20 (not shown in the figures). The peak roll and yaw rates in this stable limit-cycling spin solution can be observed from Figs. 1b and 1c to be quite large and negative, indicating a rapid left spin with nose pitched below the horizon. The average yaw rate can be estimated from Fig. 1c to be about 80 deg/s (1.4 rad/s), which gives an estimated time period of about 4 s per rotation. The pitch angle is around 17 deg (0.3 rad) below the horizon, with an angle of attack of approximately 72 deg

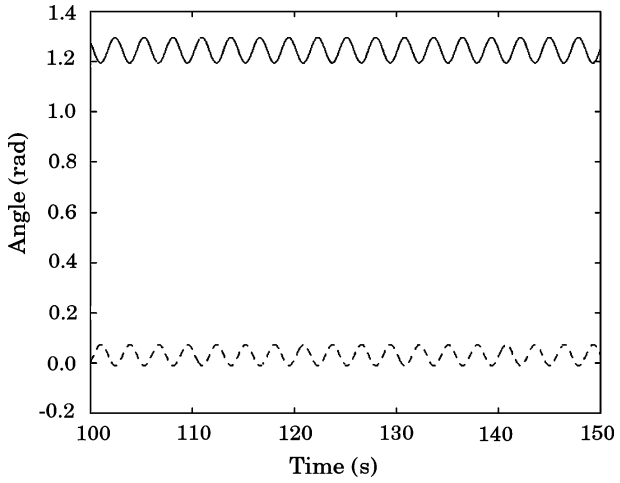

a) Angle of attack α (——) and sideslip angle β (- - - -)

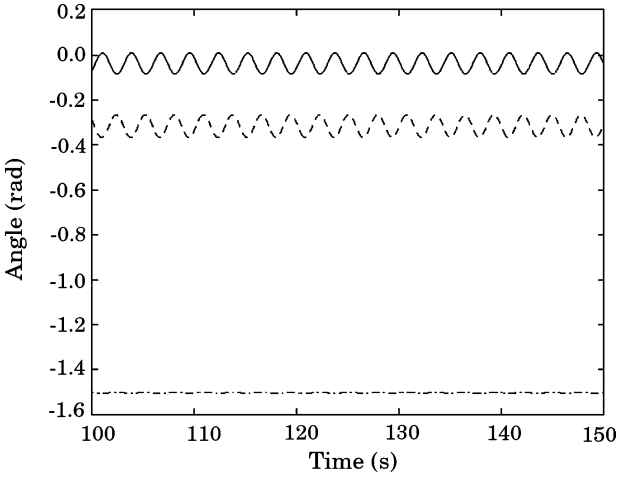

b) Roll angle ϕ (——), pitch angle θ (- - - -), and flight path angle γ (–·–)

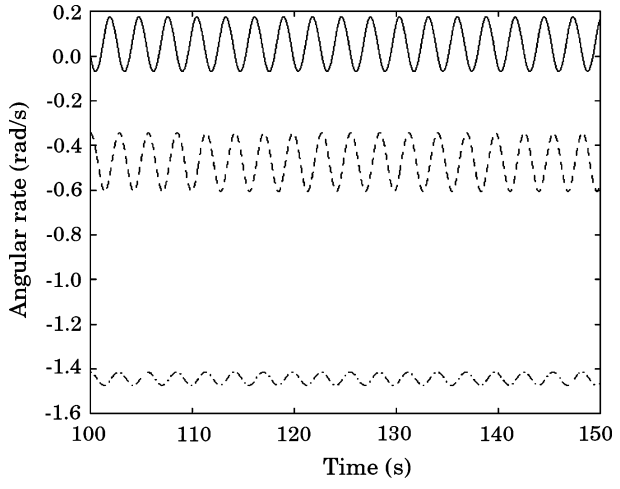

c) Roll p (- - - -), pitch q (——), and yaw r (–·–) rates

Fig. 2 Numerically simulated time histories of different state variables in fully developed oscillatory spin.

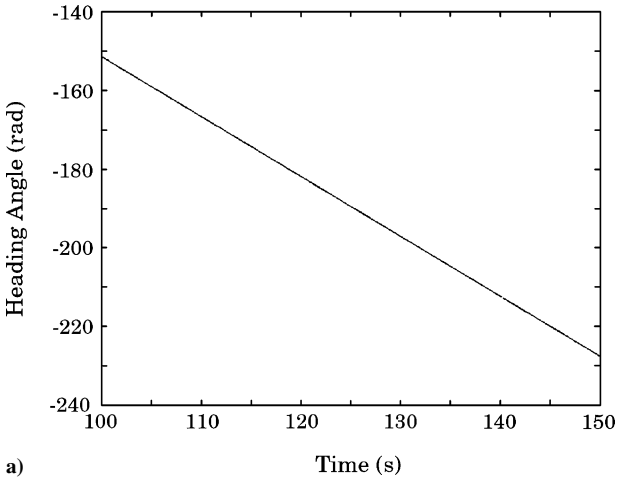

a)

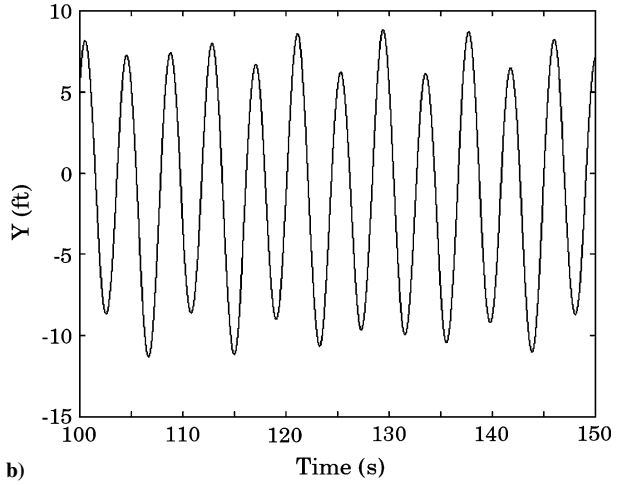

b)

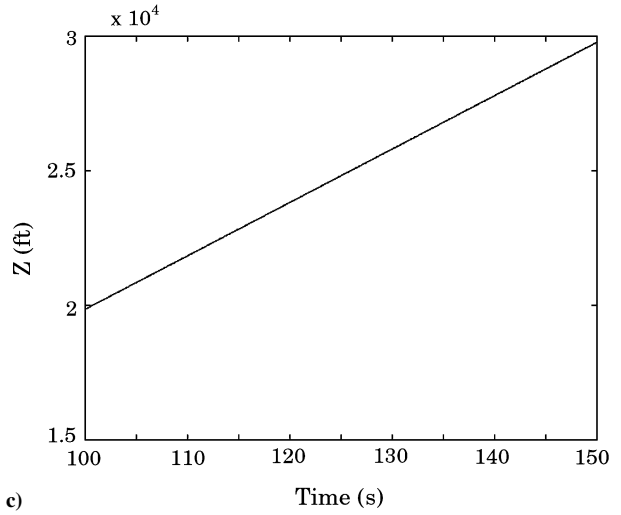

c)

Fig. 3 Numerically simulated time histories of a) heading angle ψ and position variables b) Y and c) Z in fully developed oscillatory spin.

(1.25 rad), which gives the flight-path angle to be nearly −90 deg, that is, velocity vector pointing nearly vertically downwards. The airplane therefore appears to enter a flat, oscillatory left spin at the Hopf bifurcation point H2, descending vertically with a full turn completed in around 4 s.

The oscillatory spin dynamics is numerically simulated to confirm the predictions made by the bifurcation analysis. All numerical simulations reported in this paper are carried out by using Simulink under a MATLAB® environment. The following values of the control deflections are used for this simulation:

$$\delta e = -25 \text{ deg}(-0.44 \text{ rad}), \qquad \eta = 0.38$$

$$\delta a = \delta r = \delta pv = \delta yv = 0$$

Time histories of the aircraft attitude, angular rates, and position variables in a fully developed spin over a 50-s time interval are plotted in Figs. 2 and 3. Figure 2a shows oscillations in angle of attack and sideslip angle about a mean α of about 72 deg (1.25 rad) and a mean β of 2 deg (0.035 rad). Figure 2b shows small oscillations

in roll angle about a mean left bank angle of $\phi \approx 2$ deg; consequently, the component of the angular velocity Ω about the body Y axis, that is, the pitch rate q, is also quite small, as seen in Fig. 2c. Figure 2b also shows small oscillations in pitch angle θ, while the flight-path angle γ is seen to be nearly constant at approximately -86 deg (-1.5 rad). Reasonably large negative values of roll rate are seen in Fig. 2c with a peak-to-peak variation of about 12 deg/s (0.2 rad/s), whereas the average yaw rate is very high at around -82 deg/s (-1.43 rad/s). The plot of heading angle ψ in Fig. 3a has a slope of around 1.6 rad/s, which implies that the airplane executes one turn in just under 4 s. Figure 3b reveals the radius of the turn to be of the order of 8–10 ft, whereas, from Fig. 3c, the loss in altitude can be seen to be about 200 ft per second. The oscillatory spin predicted by the bifurcation analysis and confirmed by the numerical simulation appears to match fairly well with observations on a scaled F-18/HARV model in a spin tunnel.[37]

III. Level-Flight Trim Computation

Next, the stable, level, symmetric flight trim states to which the airplane could be recovered are computed by using an EBA procedure.[31] The EBA procedure, briefly, allows the computation of equilibrium solutions subject to constraints on the state variables x_1. The aircraft dynamics given by Eq. (2) along with the constraint equations are represented in the following form:

$$\dot{\boldsymbol{x}}_1 = f_1(\boldsymbol{x}_1, u_1, u_2, \ldots, u_{m+1}, u_{m+2}, \ldots, u_r)$$
$$g_i(\boldsymbol{x}_1) = 0, \qquad i = 1, \ldots, m \tag{3}$$

where g_i are the m constraint functions; u_1 is the principal continuation parameter; $u_2, \ldots, u_{m+1}$ are the m control parameters that are to be varied as a function of u_1 so as to satisfy the constraints represented by the g_i; and $u_{m+2}, \ldots, u_r$ are the controls that are kept constant. The EBA computations are carried out in two steps. In the first step, both the state and constraint equations in Eq. (3) are solved together to simultaneously obtain the constrained equilibrium solutions $x_1(u_1)$ and the control parameter schedules $u_2(u_1), \ldots, u_{m+1}(u_1)$ required to satisfy the constraints g_i. In the second step, only the state equations in Eq. (3), with the parameter schedules computed in the first step incorporated as follows

$$\dot{\boldsymbol{x}}_1 = f_1[\boldsymbol{x}_1, u_1, u_2(u_1), \ldots, u_{m+1}(u_1), u_{m+2}, \ldots, u_r] \tag{4}$$

are solved to obtain the equilibrium states, their stability, bifurcation points, and bifurcated equilibrium branches. The equilibrium solutions on the bifurcated branches represent departures from the constrained trim states; these are valid solutions for the control parameter schedules $u_2(u_1), \ldots, u_{m+1}(u_1)$, but do not satisfy the constraints g_i.

In the present instance, the specification of level, symmetric flight trims requires the following constraints to be imposed on the flight-path angle γ, roll angle ϕ, and sideslip angle β:

$$g_1 = \gamma = 0, \qquad g_2 = \phi = 0, \qquad g_3 = \beta = 0 \tag{5}$$

The elevator deflection δe is used as the principal continuation parameter u_1, while the thrust-vectoring controls δpv and δyv are kept constant at zero. In the first step of the EBA procedure, the variation of the throttle, aileron, and rudder deflections as a function of the elevator deflection, that is to say, $\eta(\delta e)$, $\delta a(\delta e)$, and $\delta r(\delta e)$, is computed so as to satisfy the constraints in Eq. (5). The control parameter schedules thus obtained are shown in Fig. 4. Values of throttle parameter η greater than one, though nonphysical, have been computed and plotted in Fig. 4 for the purpose of contrasting recovery to trims at high angle of attack with large η against those at low angle of attack with comparatively smaller η. Figure 4 also shows notable negative deflections of aileron and rudder at large negative elevator angles required to overcome the asymmetric lateral forces/moments as a result of right and left elevator deflection and maintain level, symmetric flight.

Using the control schedules in Fig. 4, level, symmetric flight trims can be computed by the second step of the EBA procedure as in Eq. (4). Bifurcation diagrams of flight-path angle γ, roll angle ϕ, and sideslip angle β, showing level, symmetric flight trims satisfying the constraints in Eq. (5) are plotted in Figs. 5a–5c, respectively. In these figures, branches of trim solutions with nonzero γ, ϕ, and β, represent departures from the constrained trim flight condition at pitchfork/transcritical bifurcation points. The corresponding bifurcation diagram for angle of attack α as a function of elevator deflection is shown in Fig. 5d, where the three stable, level-flight trim branches of interest are marked A (high α), B (moderate α), and C (low α), respectively. The trim branch C contains the desired low α solutions with low-to-moderate throttle values to which the aircraft should recover from a spin. Branch B consists of trims at moderate α with fairly large values of throttle, in some cases even greater than one. Trims on branch B (with η less than one) could be useful as an intermediate stage in the recovery process to a low α trim state on branch C. All equilibrium solutions on branch A are unattainable as they correspond to throttle values greater than one; nevertheless, they are considered in this paper as an interesting contrast to cases B and C.

Table 1 Level-flight trim states used for spin recovery

Variable	Trim A	Trim B	Trim C
M	0.14	0.16	0.2
α	41.83 deg (0.73 rad)	28.65 deg (0.5 rad)	17.12 deg (0.3 rad)
θ	41.83 deg (0.73 rad)	28.65 deg (0.5 rad)	17.12 deg (0.3 rad)
η	1.39	0.91	0.54
δe	-8.59 deg (-0.15 rad)	-5.73 deg (-0.1 rad)	-2.86 deg (-0.05 rad)

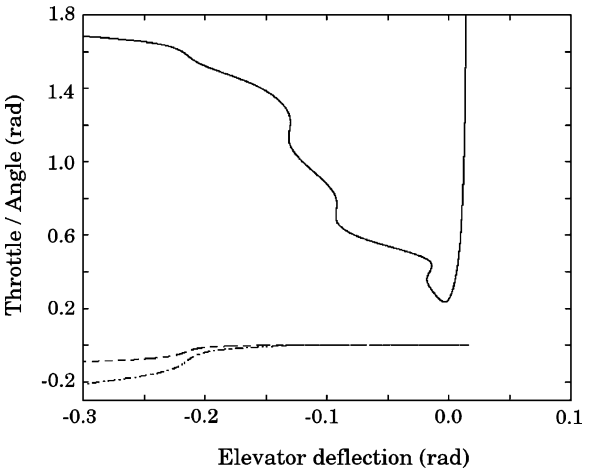

Fig. 4 Variation of throttle η (——), aileron deflection δa (- - -), and rudder deflection δr (–·–) as a function of elevator deflection δe required to maintain level, symmetric flight trims.

IV. Dynamic Inversion and Spin Recovery

In this section, spin recovery from an oscillatory spin state to one representative level trim state from each of the branches A, B, C is attempted by using a nonlinear dynamic inversion algorithm. The airplane is initially placed in the oscillatory spin state described earlier in Figs. 2 and 3 with $\delta e = -25$ deg (-0.44 rad) and $\eta = 0.38$. The control surfaces are held in position for 50 s to account for possible errors in specification of the initial conditions and to allow the airplane to settle into the spin state. The three level trim states chosen for recovery are listed in Table 1 and are themselves labeled trim A, trim B, and trim C to reflect the branch to which they belong. Variables not listed in Table 1 are to be taken to have the value zero.

A nonlinear dynamic inversion algorithm of the form proposed in Ref. 26 is implemented for spin recovery. The inversion is carried out in two loops as shown in the block diagram in Fig. 6—a fast inner

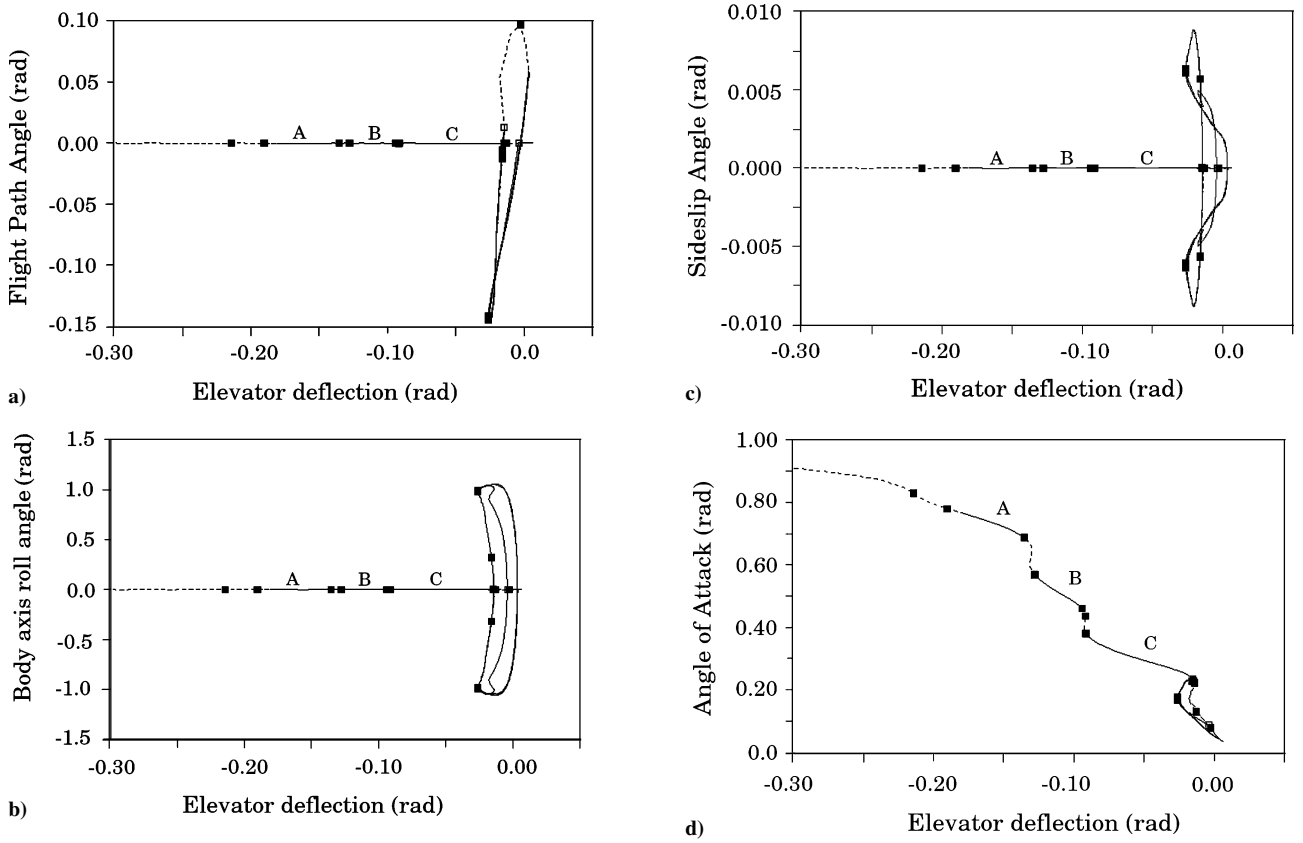

Fig. 5 Bifurcation diagram of a) flight-path angle γ, b) body-axis roll angle ϕ, c) sideslip angle β, and d) angle of attack α, with elevator deflection δe as the continuation parameter for level-flight trims: ——, stable equilibria; - - - -, unstable equilibria; ■■■, Hopf bifurcation points; and □□□, pitchfork or transcritical bifurcation points.

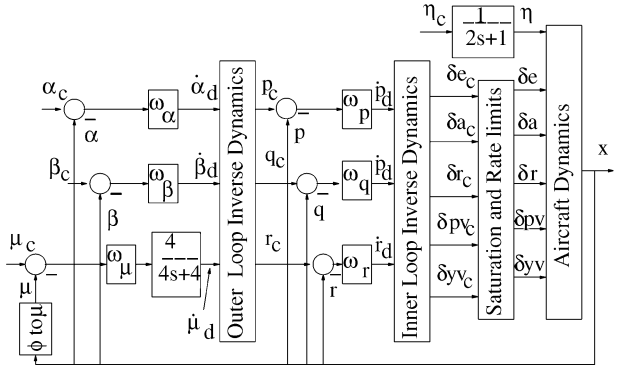

Fig. 6 Block diagram of closed-loop aircraft dynamics with the nonlinear dynamic inversion law implemented.

loop for the dynamics in the body-axis angular rates and a slow outer loop for the dynamics in the attitude angles with respect to the velocity vector. The commanded variables in the outer loop are the attitude variables: angle of attack α_c, sideslip angle β_c, and roll angle about the velocity vector μ_c. Inverting the outer-loop dynamics gives the commanded variables for the inner-loop, which are the angular rates p_c, q_c, r_c. Inversion of the inner-loop dynamics then yields the commanded values of the elevator, aileron, and rudder deflections δe_c, δa_c, and δr_c, respectively. The control surface deflections are passed through saturation and rate limiter blocks before being input to the aircraft dynamics. The thrust-vectoring controls are not commanded in this phase of the study; both δpv and δyv are kept unchanged at zero. It is assumed that all of the aircraft states are available for feedback to compute the dynamic inversion laws. The bandwidths $\omega_p, \omega_q, \omega_r$ along the roll, pitch, and yaw rate paths in the inner loop are all taken to be 10 rad/s. In the outer loop, the bandwidths $\omega_\alpha, \omega_\beta$ in the angle of attack and sideslip angle paths are set to 2 rad/s, $\omega_\mu = 1.5$ rad/s, and a ± 2.5 rad/s limit (not shown in Fig. 6) is imposed on the roll rate command, which is then passed through a filter $4/(s+4)$. The ratio between the outer- and inner-loop bandwidths, which is of the order of 1:5, ensures that the coupling between the two loops is minimized though not entirely eliminated. Throttle commands η_c are passed through a filter $1/(2s+1)$, which models the lag in the throttle response.

The dynamic inversion algorithm just described is next used for spin recovery to the three level trim states labeled A, B, C in Table 1. In each case, commanded values of angle of attack, sideslip, roll angle, and throttle are given as step commands at $t = 50$ s; the value of α_c and η_c for the three cases is as listed in Table 1, whereas β_c and μ_c are zero in all three cases. Time histories of angle of attack α, sideslip angle β, and body-axis roll angle ϕ, for the three cases of recovery to trims A, B, C, are shown in Figs. 7a, 8a, and 8b, respectively. It is seen that in each case the commanded angle of attack is achieved, whereas $\beta_c = 0$ and $\mu_c = 0$ (equivalently, $\phi = 0$) are obtained only in case of trims A and B. The third case shows a wing rock-like limit-cycle oscillation in the lateral variables about the specified values for trim C; this was found to be caused by the presence of the rate limiter in the rudder deflection path. It can be noticed from Fig. 7a that oscillations in α about trim A are poorly damped as compared to the case of trim B; the reason for this can be traced to limits on the elevator deflection coupled with the lag in throttle response. Both lateral and longitudinal variables can be seen to settle down to the trim B values in about 20 s from the point of application of recovery controls at $t = 50$ s; whereas for trim A the lateral variables take about 30 s for recovery while the angle of attack requires nearly 40 s to reach the trim value. The phugoid mode, which is uncontrolled, has a larger timescale but is damped in all three cases, as seen in Fig. 7b, which shows that zero flight-path angle γ is fairly well achieved in every case, that is, the airplane is always recovered from spin to level flight. However, the desired trim state is reached only in cases A and B; recovery to trim C results in the airplane ending up in a rate-limiter-induced limit-cycle oscillation about the trim state C.

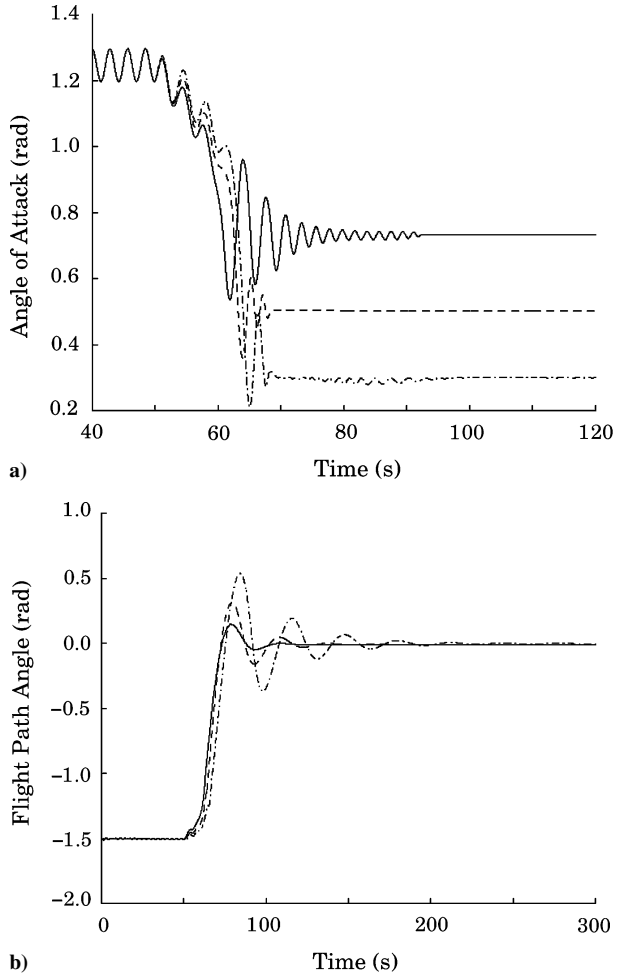

Fig. 7 Time history of a) angle of attack α and b) flight-path angle γ, during spin recovery to trim A (——), trim B (- - - -), and trim C (–·–), using the dynamic inversion law in Fig. 6.

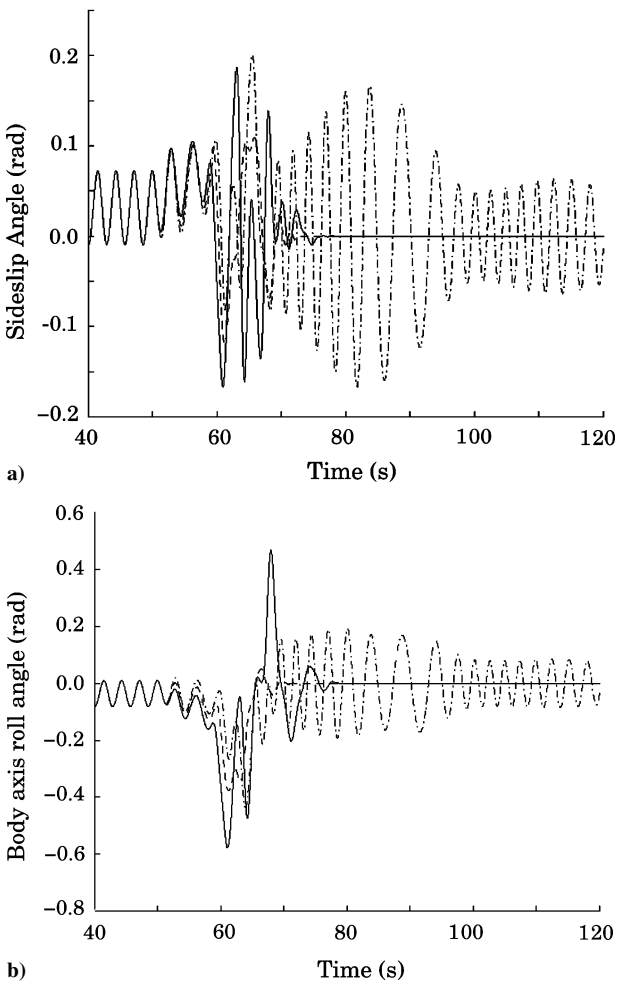

Fig. 8 Time history of a) sideslip angle β and b) body-axis roll angle ϕ, during spin recovery to trim A (——), trim B (- - - -), and trim C (–·–), using the dynamic inversion law in Fig. 6.

It is of interest to examine the control inputs given to the airplane during the recovery process. The throttle input, shown in Fig. 9a, takes of the order of 10 s to reach the respective commanded value η_c, reflecting the time lag in the throttle loop of $T_s = 2$ s. The elevator, aileron, and rudder inputs in Figs. 9b, 10a, and 10b reveal that the spin recovery strategy of the dynamic inversion law is to apply aileron with the roll, rudder against the turn, and elevator to pitch the nose down. All three controls, in all three cases A, B, C, are applied simultaneously at $t = 50$ s at the maximum rate permitted by the rate limiter and to the maximum value limited by saturation; what is different between the three cases is the point of time at which the controls are withdrawn from their maximum saturated values. For example, Fig. 9b shows that the maximum down-elevator deflection of 10 deg (0.175 rad) is released at $t \approx 61$ s for case A, 2 s later for case B, and another 1–2 s later for case C. These times roughly coincide with the moments at which the corresponding α graphs in Fig. 7a first cross the respective commanded values α_c. Similar observations can be made for the rudder and aileron inputs as well. Beyond that point, the control deflections aim to provide the desired level of stability (damping and frequency) in the pitch, roll, and yaw loops. Thus, in cases where the aerodynamic damping and/or control effectiveness is presumably lower, the commanded control deflections are larger, and the control inputs show more severe oscillations. For instance, the elevator deflection in Fig. 9b for case A shows continued fluctuations between the upper and lower saturation limits indicating that the elevator input required to obtain the desired level of damping exceeds the limiting values. Thus, these fluctuations in elevator input can be correlated to the poorly damped oscillations in angle of attack about trim A in Fig. 7a. In case C, the commanded rudder deflections seem to exceed the saturation limits, and consequently Fig. 10b shows persistent oscillations in the rudder input between the upper and lower saturation values of ± 30 deg (± 0.52 rad) with rate-limited transitions between them. This induces oscillations in all of the lateral variables (see Figs. 8a and 8b for β and ϕ), in the aileron input (Fig. 10a), and also in the elevator deflection (Fig. 9b); however, the oscillations in the longitudinal variables α and γ (see Figs. 7a and 7b) are too small to be apparent in the figures. When the rate limit of ± 82 deg/s in the rudder loop is sufficiently relaxed, these oscillations disappear, and recovery to trim C becomes possible.

In summary, the airplane recovers to trim A ($\alpha = 41.83$ deg) in nearly 40 s, to trim B ($\alpha = 28.65$ deg) in about 20 s, but recovery to trim C ($\alpha = 17.12$ deg) leaves the airplane in a wing rock-like limit-cycle oscillation about the trim state. The initial application of aileron and rudder for spin recovery is along conventional lines for a low-aspect-ratio, fuselage-heavy configuration, but what is notable is the simultaneous use of elevator and throttle, the withdrawal of the recovery controls at a precise moment, and the further vigorous use of controls to damp out residual oscillations. In particular, opening the throttle picks up the velocity vector (makes the flight-path angle less negative) at the same time as the elevator pitches the nose down, which together help attain the commanded angle of attack as quickly as possible. The influence of throttle on the angle of attack is apparent in Fig. 7a, where starting from the same initial condition and with the same elevator input for $t = 50$–61 s the aircraft response at the end of 61 s for different throttle inputs is different, as follows: $\alpha \approx 0.7$ rad for case A ($\eta_c = 1.39$); $\alpha \approx 0.9$ rad for case B ($\eta_c = 0.91$); $\alpha \approx 1.0$ rad for case C ($\eta_c = 0.54$).

In the following sections, we examine two different strategies to recover the airplane from oscillatory spin to the low-angle-of-attack

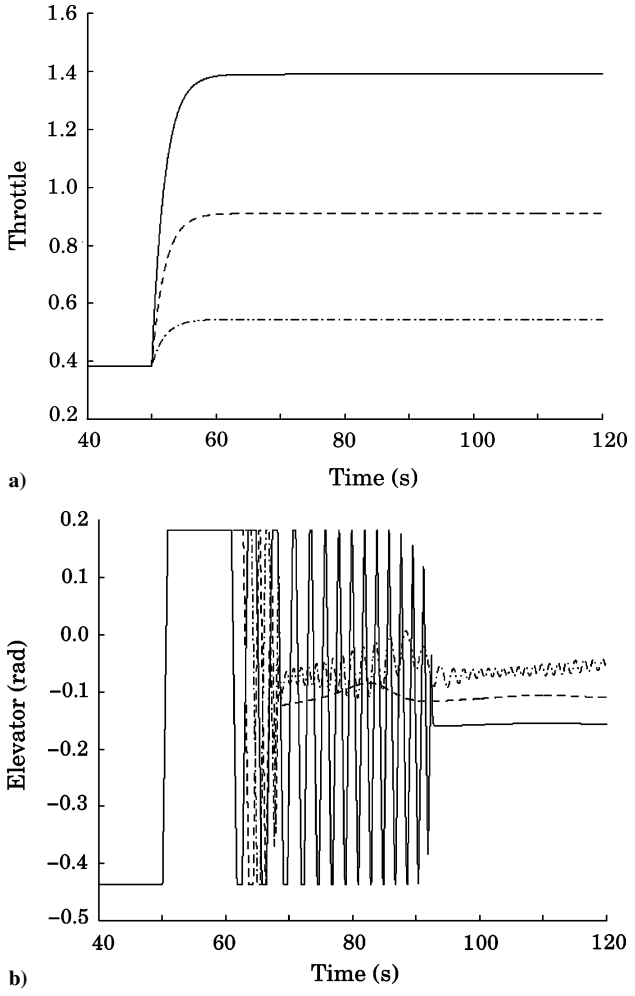

Fig. 9 Time history of a) throttle input η and b) elevator input δe, during spin recovery to trim A (——), trim B (- - - -), and trim C (–·–), using the dynamic inversion law in Fig. 6.

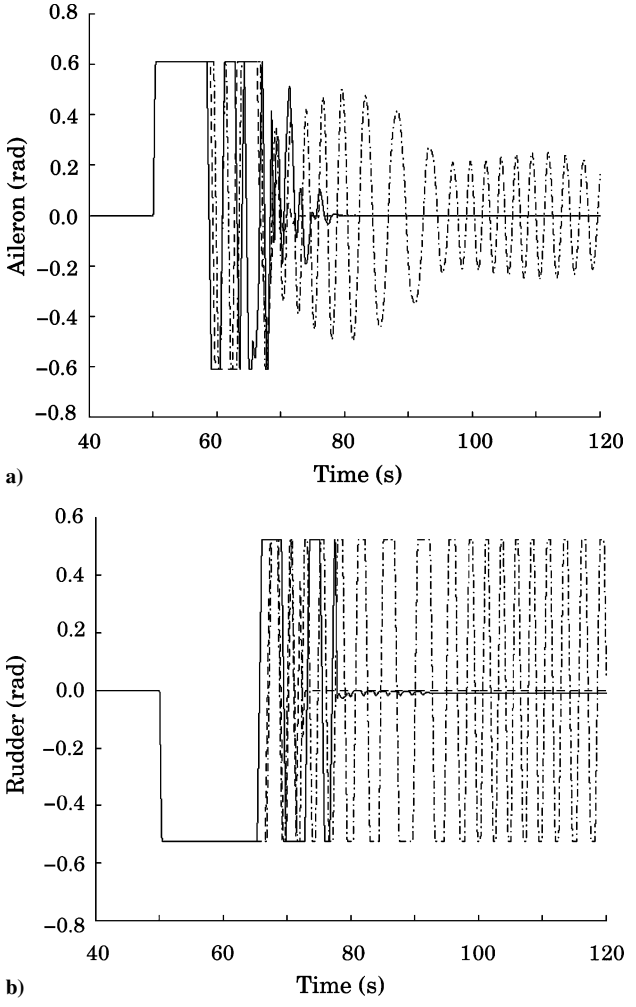

Fig. 10 Time history of a) aileron input δa and b) rudder input δr, during spin recovery to trim A (——), trim B (- - - -), and trim C (–·–), using the dynamic inversion law in Fig. 6.

trim state C without encountering the limit-cycle oscillations just seen.

V. Two-Step Spin Recovery

Simulations in the preceding section have shown that recovery to trim B is physically possible ($\eta < 1$) in a time of about 20 s. This raises the possibility that recovery to trim C without encountering the rate-limiter-induced limit-cycle oscillations can be achieved by using trim B as an intermediate state in the recovery process. To test this hypothesis, starting from the same oscillatory spin state as before, recovery controls are applied by commanding values of α_c and η_c corresponding to trim B, and β_c and μ_c equal to zero (common to trims B and C). All commands are applied as step functions at $t = 50$ s. After 20 s of recovery, that is, at $t = 70$ s, α_c and η_c are commanded to the values corresponding to trim C, again as step functions. Figure 11 shows α briefly settling into the trim B value before further decreasing in response to the step forcing at 70 s to finally settle down to the correct trim C value. Sideslip β and roll angle ϕ are also seen from Fig. 11 to attain the desired zero value, and so do all of the other state variables not shown in the figure. Thus, the two-step procedure is successful in recovering the airplane to trim C in a little less than 25 s.

Figures 12a and 12b show the control surface deflections and the throttle movement during the two-step recovery procedure. The initial control deflections are, of course, identical to those in the trim B case in the preceding section; however, at $t = 70$ s an additional downelevator deflection is given to decrease α from 28 deg at trim B to 17 deg at trim C. Both β and ϕ are already fairly close to zero at the end of $t = 70$ s, and no abrupt variation in aileron and rudder inputs is noticed in Fig. 12b during the transition from trim B to C. What is significant is the change in throttle in Fig. 12a: first an increase at $t = 50$ s from 0.38 at spin to 0.91 for trim B, then a decrease to the trim C value of 0.54 initiated at $t = 70$ s. This variation of throttle, along with the two-step α_c command, is seen to be critical to successful spin recovery to trim C. For instance, if the throttle were merely increased from 0.38 to the trim C value of 0.54 initially and then held constant while the two-step α_c command was applied as before, the airplane would enter the limit-cycle oscillations about trim C observed earlier. This result highlights the importance of effective use of throttle along with suitably timed elevator deflections, in addition to standard recovery aileron and rudder inputs, to transition an aircraft successfully from spin to a low-angle-of-attack, level trim flight.

In the recovery process to a low-α level trim state C, it is not necessary for the intermediate, transitory state B to correspond to a level-flight solution. It is possible to find several stable, equilibrium states with the same angle of attack as trim B, but corresponding to nonlevel (ascending or descending) flights with nonzero values of γ. Any of these solutions can be chosen as the intermediate state during spin recovery to trim C, with the same intermediate value of the commanded angle of attack α_c, but with a suitably different choice of η_c.

Conventional practice, which requires only aileron and rudder inputs to be applied initially for spin recovery, means that the rudder needs to produce sufficiently strong antispin yawing moments, typically under unfavorable flight regimes at high angles of attack, where aerodynamic damping and stability are low and control effectiveness is limited. In contrast, the two-step recovery procedure

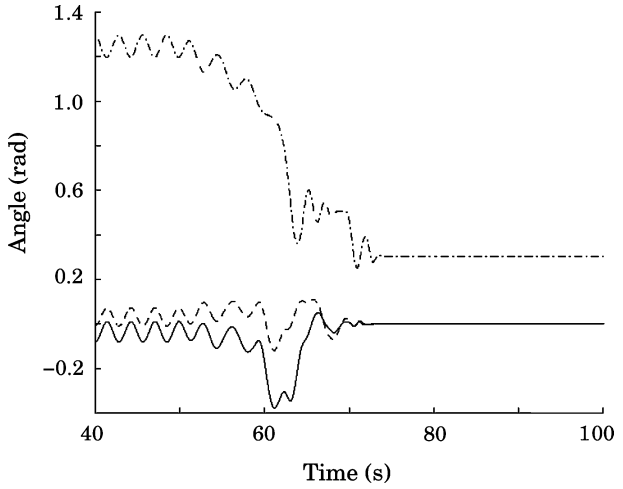

Fig. 11 Time history of angle of attack α (–·–), sideslip angle β (- - - -), and body-axis roll angle ϕ (——) during the two-step spin recovery to trim C.

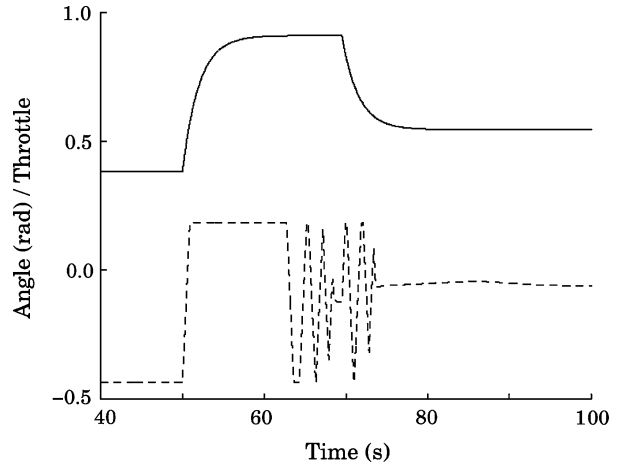

a) Elevator input δe (- - - -) and throttle η (——)

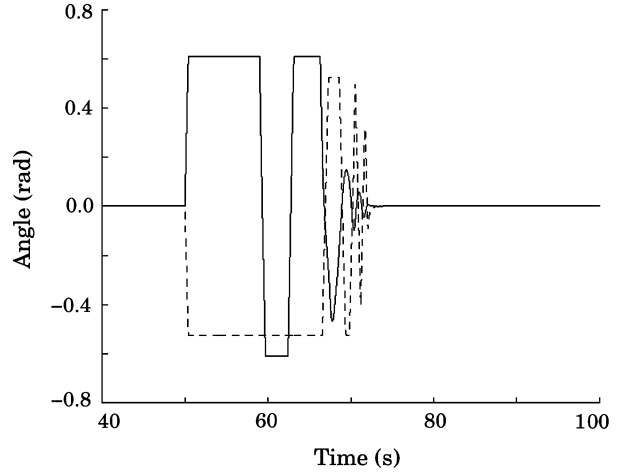

b) Aileron input δa (——) and rudder input δr (- - - -)

Fig. 12 Time history of aerodynamic control inputs and throttle during the two-step spin recovery to trim C.

discussed here uses elevator and throttle inputs, simultaneously with the aileron and rudder controls, to reduce the angle of attack to a favorable intermediate flight condition. This intermediate trim state can be selected to be one where aerodynamic stiffness and damping effects, especially in the lateral-directional modes, as well as rudder effectiveness are relatively stronger, thus aiding in quickly stopping the spin rotation. Of course, elevator effectiveness can itself be restricted at the high angles of attack characteristic of spin and might need to be supplemented by other control effectors. Additionally, gyroscopic effects caused by simultaneous, large roll, pitch, and yaw rates, might need to be opposed by increased control moments. The use of increased throttle as a means to speed up the reduction in angle of attack has been explored in this section and has been seen to be effective; however, the lag in the throttle response is an important limiting factor in the recovery time. The use of thrust vectoring to supplement the aerodynamic controls at high angles of attack might be helpful in further reducing the recovery time; this is the subject matter of the next section.

VI. Spin Recovery with Thrust Vectoring

Two additional control effectors, pitch thrust vector deflection δpv and yaw thrust vector deflection δyv, are now considered. Simulations for spin recovery are carried out using the same dynamic inversion algorithm as before (Fig. 6), except that the inner-loop inverse dynamics block is used to compute all five control commands as against three earlier. The pitch and yaw thrust-vectoring commands are computed by using a daisychaining algorithm,[38] as shown in Fig. 13 and explained next. The dashed box bounding Fig. 13 represents the inner-loop inverse dynamics block in Fig. 6 with the three angular acceleration demands as input and the five control deflection commands as output. Within this box, the first block inverts the dynamics in the angular rates to compute the control moments required in the three paths L_c, M_c, N_c. The next block uses the desired control moments L_c, M_c, N_c to compute the commanded values of the aerodynamic controls δe_c, δa_c, δr_c, which are available as outputs. To compute the pitch and yaw thrust-vector commands, the pitch and yaw control moments M_a, N_a, obtained from the aerodynamic control deflections available, subject to rate and position limits, are compared with the desired values of the pitch and yaw control moments M_c, N_c, respectively. If either of the aerodynamic control moments in pitch/yaw is inadequate, the additional moment required, $M_c - M_a = M_{\text{tv}}$, $N_c - N_a = N_{\text{tv}}$, is sought from the appropriate thrust-vector deflection. The corresponding values of pitch and yaw thrust-vector deflections δpv_c, δyv_c are calculated and are provided as outputs from the block. No contribution of thrust vectoring to the roll moment is modeled. All of the five control commands are then passed through position and rate limiter blocks before being input to the aircraft dynamics, as shown in Fig. 6.

Once again, starting at the same oscillatory spin state as before, recovery commands are given as step functions at $t = 50$ s, with values corresponding to trim C, as follows: $\alpha_c = 0.3$ rad, $\eta_c = 0.54$, $\beta_c = 0$, and $\mu_c = 0$. All of the state variables do recover to the trim C values, and the variation of α, β, and ϕ, plotted in Fig. 14, shows the recovery time to be around 10 s. Figure 15a shows the elevator and pitch thrust vector inputs given to the airplane. It is seen that the initial full downelevator (positive) deflection is supplemented by full downnozzle (positive) deflection, thereby providing additional nose-down pitching moment. The first crossing of $\alpha_c = 0.3$ rad in Fig. 14 therefore occurs at $t = 55$ s as against $t = 61$ s in the non-thrust-vectored case. Even after the elevator deflection ceases to be

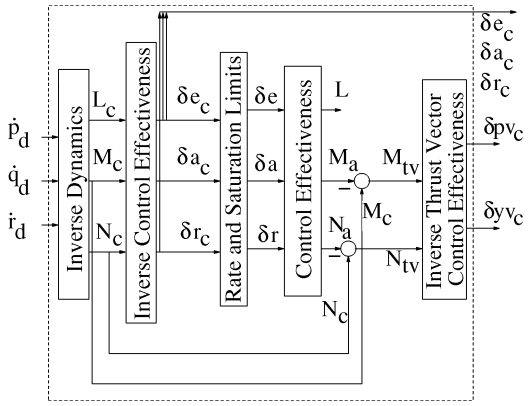

Fig. 13 Block diagram of the daisychaining algorithm to compute the thrust-vectoring commands.

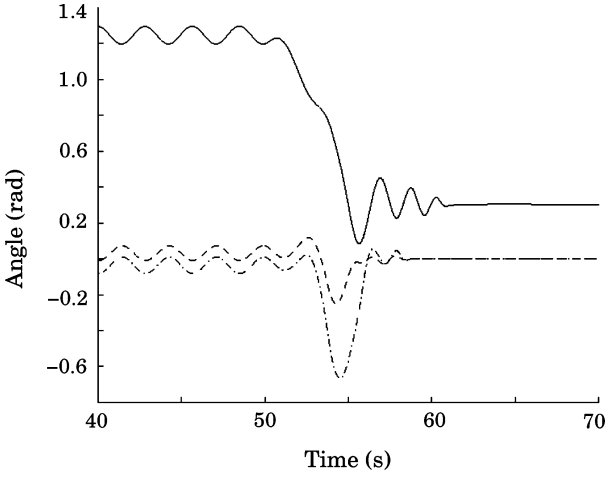

Fig. 14 Time history of angle of attack α (——), sideslip angle β (- - - -), and body-axis roll angle ϕ (–·–·–) during spin recovery to trim C with thrust vectoring.

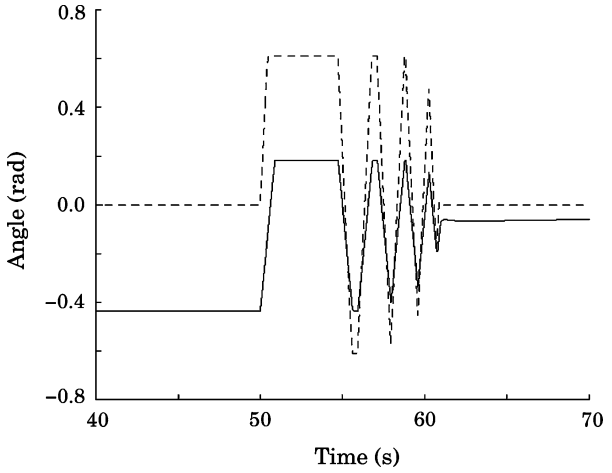

a) Elevator input δe (——) and pitch thrust vector input δpv (- - - -)

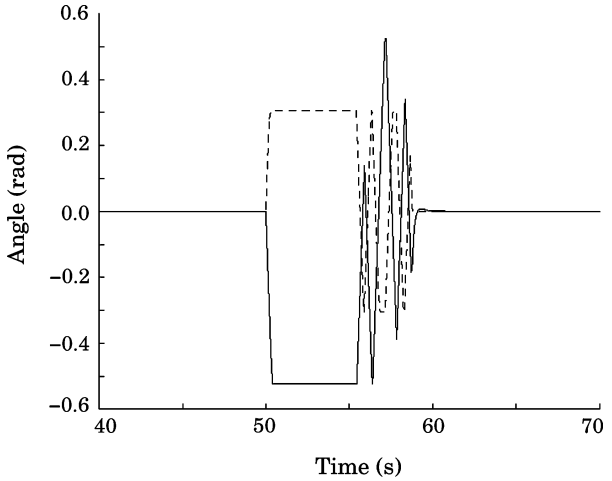

b) Rudder input δr (——) and yaw thrust vector input δyv (- - - -)

Fig. 15 Time history of control inputs in pitch and yaw axes during spin recovery to trim C with thrust vectoring.

position limited, the pitch thrust-vectoring command is still active to overcome the shortfall in the required pitch control moment as a result of elevator rate limiting. Figure 15b shows a similar trend where the initial full right (negative) rudder deflection is supplemented by full right nozzle (positive) deflection, which together provide the desired antispin yawing moments to arrest the rotation. The aileron and throttle inputs are not remarkable in themselves and have therefore not been plotted here. It is clear that the use of thrust vectoring provides a powerful additional source of pitch/yaw moments that is useful, especially at high angles of attack, to apply the large control moments that are required to recover from spin to a low-α level trim state. However, as pointed out previously,[33] it is important to apply the thrust-vectoring commands in a precise manner (e.g., withdrawal at the correct point of time) to avoid pushing the airplane into another extreme flight condition. The dynamic inversion algorithm employed in the present study is seen to be an effective strategy for commanding the thrust-vector (and other control) commands during a complicated, nonlinear maneuver such as that during spin recovery.

VII. Conclusions

The problem of recovering an aircraft from a flat, oscillatory spin has been posed as an inverse dynamics problem of computing the control inputs required to transition the airplane from the spin state to a symmetric, level-flight trim condition. The use of bifurcation analysis, in conjunction with the nonlinear dynamic inversion method, has been critical as it provided both the start point (oscillatory spin solution) as well the endpoint (stable, level flight trim solution) for the inversion algorithm. Three different level-flight trims have been examined, which represent high-, moderate-, and low-angle-of-attack α trims for the aircraft model under consideration. Spin recovery, using only aerodynamic control surfaces, is seen to be successful in case of the high- and moderate-α trims, but leaves the airplane in a wing rock-like limit-cycle oscillation about the low-α trim state. Two alternate strategies—one involving a two-step recovery procedure using only aerodynamic controls and the other using additional thrust vector control effectors—are both seen to be successful in recovering the airplane to the low-α trim state. Some interesting observations can be made as a result of these simulations, as follows:

1) Recovery to high-α trims is not necessarily faster as the poor aerodynamic damping under these conditions implies that residual oscillations do not decay rapidly. Even the control surfaces, under full deflection conditions, are unable to provide sufficient damping augmentation. As a result, the airplane takes nearly twice as long to recover to high-α trim A than to the moderate-α trim B. Hence, stabilization at a high-α trim, as in Refs. 19 and 34, might not always be recommended.

2) Direct recovery from a flat spin to a low-α trim, such as trim C, is not to be expected because of control surface rate and deflection limits. One can consider switching off the dynamic inversion controller or switching to an alternate control strategy at a particular point in time to try avoiding the rate-limiter-induced limit cycle in case of trim C. This needs further exploration, however.

3) The two-step spin recovery strategy is a practical possibility for aircraft not equipped with thrust vectoring. The intermediate trim state, such as trim B, can be chosen to have good stability and damping characteristics and adequate control effectiveness, especially in the lateral-directional dynamics. The use of increased thrust, something that used to be practiced in the early days of aviation, is seen to be an important factor in the success of the two-step recovery procedure. However, the use of throttle input during spin recovery, in general, needs to be carefully evaluated.

4) Further simulations using pitch and yaw thrust vectoring have shown that airplanes equipped with thrust vectoring have a distinct advantage in being able to recover from flat spin directly to a low-α trim. In the example considered here, spin recovery time was reduced by a factor of nearly 60% for a thrust-vectored airplane, as against the same airplane without thrust vectoring undergoing a two-step spin recovery procedure. More extensive simulations should be able to better quantify the precise advantage gained in spin recovery by incorporating thrust vectoring when additional factors such as thrust/weight penalty caused by addition of thrust-vectoring nozzles are considered.

5) Finally, all of the simulations show that the initial sense of application of recovery controls is very much along expected lines—aileron with the roll, rudder/yaw thrust vectoring against the turn, and elevator/pitch thrust vectoring to pitch the nose down to a lower angle of attack. Most importantly, the dynamic inversion

algorithm is able to precisely time the withdrawal of each control input, and this turns out to be crucial to a well-timed spin recovery. Failure on this count could, as seen in Ref. 33, result in the airplane ending up in another extreme flight condition, such as transitioning from a left spin to a right spin.

Appendix A: Aircraft Equations and Data

The complete six-degree-of-freedom dynamics of a rigid airplane in flight is described by the following set of 12, coupled, nonlinear, first-order differential equations[29]:

$$\dot{V} = \frac{1}{m}\left[T_m \eta \cos\alpha \cos\beta - \frac{1}{2} C_D(\alpha, q, \delta e, \delta pv)\rho V^2 S - mg \sin\gamma\right]$$

$$\dot{\alpha} = q - \frac{1}{\cos\beta}\left\{(p\cos\alpha + r\sin\alpha)\sin\beta + \frac{1}{mV}\left[T_m \eta \sin\alpha + \frac{1}{2} C_L(\alpha, q, \delta e, \delta pv)\rho V^2 S - mg\cos\mu\cos\gamma\right]\right\}$$

$$\dot{\beta} = \frac{1}{mV}\left[-T_m \eta \cos\alpha \sin\beta + \frac{1}{2} C_Y(\beta, p, r, \delta e, \delta a, \delta r, \delta yv)\rho V^2 S + mg \sin\mu\cos\gamma\right] + (p\sin\alpha - r\cos\alpha) \tag{A1}$$

$$\dot{p} = \frac{I_y - I_z}{I_x} qr + \frac{1}{2I_x}\rho V^2 SbC_l(\beta, p, r, \delta e, \delta a, \delta r, \delta yv)$$

$$\dot{q} = \frac{I_z - I_x}{I_y} pr + \frac{1}{2I_y}\rho V^2 ScC_m(\alpha, q, \delta e, \delta pv)$$

$$\dot{r} = \frac{I_x - I_y}{I_z} pq + \frac{1}{2I_z}\rho V^2 SbC_n(\beta, p, r, \delta e, \delta a, \delta r, \delta yv) \tag{A2}$$

$$\dot{\phi} = p + q\sin\phi\tan\theta + r\cos\phi\tan\theta$$

$$\dot{\theta} = q\cos\phi - r\sin\phi, \qquad \dot{\psi} = \frac{(q\sin\phi + r\cos\phi)}{\cos\theta} \tag{A3}$$

$$\dot{X} = V\cos\gamma\cos\chi, \qquad \dot{Y} = V\cos\gamma\sin\chi, \qquad \dot{Z} = -V\sin\gamma \tag{A4}$$

The angles μ, γ, and χ in Eqs. (A1) and (A4) are defined as follows:

$$\sin\gamma = \cos\alpha\cos\beta\sin\theta - \sin\beta\sin\phi\cos\theta - \sin\alpha\cos\beta\cos\phi\cos\theta$$

$$\sin\mu\cos\gamma = \sin\theta\cos\alpha\sin\beta + \sin\phi\cos\theta\cos\beta - \sin\alpha\sin\beta\cos\phi\cos\theta$$

$$\cos\mu\cos\gamma = \sin\theta\sin\alpha + \cos\alpha\cos\phi\cos\theta$$

$$\sin\chi\cos\gamma = \cos\alpha\cos\beta\cos\theta\sin\psi + \sin\beta(\sin\phi\sin\theta\sin\psi + \cos\phi\cos\psi) + \sin\alpha\cos\beta(\cos\phi\sin\theta\sin\psi - \sin\phi\cos\psi) \tag{A5}$$

The control surface deflections and thrust-vectoring nozzles are taken to have position and rate limits as listed in Table A1. No rate limit is explicitly modeled for the throttle parameter; instead, a first-order filter $1/(2s+1)$ is used to model the lag in the throttle response.

The values of the various constants in the model are as reported in Table A2. The six aerodynamic coefficients in Eqs. (A1) and (A2) are modeled in the usual manner. Each coefficient is obtained as a sum of terms, where each term is the product of a nondimensional stability/control derivative with the appropriate nondimensional state or control variable. A list of stability/control derivatives used in this study is provided in Table A3. Each entry in Table A3 is available as a function of angle of attack α in tabular form at intervals of 4 deg over a range of α from -14 deg to 90 deg. These data are available in the public domain* with additional data from Refs. 39 and 40.

Table A1 Control surface position and rate limits

Control	Symbol	Position limits, deg	Rate limits, deg/s
Elevator deflection	δe	$(-25, 10)$	± 40
Aileron deflection	δa	$(-35, 35)$	± 100
Rudder deflection	δr	$(-30, 30)$	± 82
Throttle parameter	η	$(0, 1)$	None
Pitch thrust vectoring	δ_{pv}	$(-35, 35)$	± 80
Yaw thrust vectoring	δ_{yv}	$(-17.5, 17.5)$	± 80

Table A2 Aircraft model data

Quantity	Value
Wing span b	37.42 ft
Mean aerodynamic chord c	11.52 ft
Gravitational acceleration g	32.0 ft/s^2
Roll inertia I_x	22789 slug $-$ ft^2
Pitch inertia I_y	176809 slug $-$ ft^2
Yaw inertia I_z	191744 slug $-$ ft^2
Aircraft mass m	1128.09 slug
Wing area S	400 ft^2
Maximum thrust T_m	16000 lb
Density of air ρ	0.00258 slug/ft^3

Table A3 List of nondimensional stability/control derivatives used to model the aerodynamic force and moment coefficients

	Derivative in					
With respect to	Pitch	Lift	Drag	Roll	Yaw	Side force
Angle of attack	C_{m_0}	C_{L_0}	C_{D_0}	——	——	——
Sideslip angle	——	——	——	C_{l_β}	C_{n_β}	C_{y_β}
Pitch rate	C_{m_q}	C_{L_q}	C_{D_q}	——	——	——
Roll rate	——	——	——	C_{l_p}	C_{n_p}	C_{y_p}
Yaw rate	——	——	——	C_{l_r}	C_{n_r}	C_{y_r}
Right elevator	$C_{m_{\delta er}}$	$C_{L_{\delta er}}$	$C_{D_{\delta er}}$	$C_{l_{\delta er}}$	$C_{n_{\delta er}}$	$C_{y_{\delta er}}$
Left elevator	$C_{m_{\delta el}}$	$C_{L_{\delta el}}$	$C_{D_{\delta el}}$	$C_{l_{\delta el}}$	$C_{n_{\delta el}}$	$C_{y_{\delta el}}$
Aileron	——	——	——	$C_{l_{\delta a}}$	$C_{n_{\delta a}}$	$C_{y_{\delta a}}$
Rudder	——	——	——	$C_{l_{\delta r}}$	$C_{n_{\delta r}}$	$C_{y_{\delta r}}$
Pitch thrust vectoring	$C_{m_{\delta pv}}$	$C_{L_{\delta pv}}$	$C_{D_{\delta pv}}$	——	——	——
Yaw thrust vectoring	——	——	——	$C_{l_{\delta yv}}$	$C_{n_{\delta yv}}$	$C_{y_{\delta yv}}$

References

[1] Mason, S., *Stalls, Spins, and Safety*, McGraw–Hill, New York, 1982.

[2] DeLacerda, F. G., *Facts About Spins*, 2nd ed., Iowa State Univ. Press, Ames, IA, 2002.

[3] Abzug, M. J., and Larrabee, E. E., *Airplane Stability and Control—A History of the Technologies That Made Aviation Possible*, Cambridge Univ. Press, Cambridge, England, U.K., 1997, pp. 115–139.

[4] Tischler, M. B., and Barlow, J. B., "Determination of the Spin and Recovery Characteristics of a General Aviation Design," *Journal of Aircraft*, Vol. 18, No. 4, 1981, pp. 238–244.

[5] Bihrle, W., Jr., and Barnhart, B., "Spin Prediction Techniques," *Journal of Aircraft*, Vol. 20, No. 2, 1983, pp. 97–101.

[6] Kimberlin, R. D., *Flight Testing of Fixed-Wing Aircraft*, AIAA Education Series, AIAA, Reston, VA, 2003, pp. 383–416.

[7] Carroll, J. V., and Mehra, R. K., "Bifurcation Analysis of Nonlinear Aircraft Dynamics," *Journal of Guidance, Control, and Dynamics*, Vol. 5, No. 5, 1982, pp. 529–536.

[8] Zagaynov, G. I., and Goman, M. G., "Bifurcation Analysis of Critical Aircraft Flight Regimes," ICAS Paper 84-4.2.1, Anaheim, CA, 1984.

*Data available online at http://www.dfrc.nasa.gov/Research/HARV/Work/NASA2/nasa2.html.

[9]Goman, M. G., Zagaynov, G. I., and Khramtsovsky, A. V., "Application of Bifurcation Methods to Nonlinear Flight Dynamics Problems," *Progress in Aerospace Sciences*, Vol. 33, No. 59, 1997, pp. 539–586.

[10]Sinha, N. K., "Application of Bifurcation Methods to Nonlinear Flight Dynamics," *Journal of the Aeronautical Society of India*, Vol. 53, No. 4, 2001, pp. 253–270.

[11]Planeaux, J. B., and Barth, T. J., "High-Angle-of-Attack Dynamic Behavior of a Model High-Performance Fighter Aircraft," AIAA Paper 1988-4368, Aug. 1988.

[12]Guicheteau, P., "Bifurcation Theory in Flight Dynamics—An Application to a Real Combat Aircraft," ICAS Paper 90-5.10.4, Stockholm, 1990.

[13]Goman, M., Khramtsovsky, A., Soukhanov, V., Syrovatsky, V., and Tatarnikov, K., "Aircraft Spin Prevention/Recovery Control System," TsAGI, Nov. 1993.

[14]Ananthkrishnan, N., and Sudhakar, K., "Prevention of Jump in Inertia-Coupled Roll Maneuvers of Aircraft," *Journal of Aircraft*, Vol. 31, No. 4, 1994, pp. 981–983.

[15]Lowenberg, M. H., "Development of Control Schedules to Modify Spin Behavior," AIAA Paper 1998-4267, Aug. 1998.

[16]Littleboy, D. M., and Smith, P. R., "Using Bifurcation Methods to Aid Nonlinear Dynamic Inversion Control Law Design," *Journal of Guidance, Control, and Dynamics*, Vol. 21, No. 4, 1998, pp. 632–638.

[17]Jahnke, C. C., and Culick, F. E. C., "Application of Bifurcation Theory to the High-Angle-of-Attack Dynamics of the F-14," *Journal of Aircraft*, Vol. 31, No. 1, 1994, pp. 26–34.

[18]Goman, M. G., and Khramtsovsky, A. V., "Application of Continuation and Bifurcation Methods to the Design of Control Systems," *Philosophical Transactions of the Royal Society of London Series A—Mathematical, Physical, and Engineering Sciences*, Vol. 356, No. 1745, 1998, pp. 2277–2295.

[19]Saraf, A., Deodhare, G., and Ghose, D., "Synthesis of Nonlinear Controller to Recover an Unstable Aircraft from Poststall Regime," *Journal of Guidance, Control, and Dynamics*, Vol. 22, No. 5, 1999, pp. 710–717.

[20]Kato, O., and Sugiura, I., "An Interpretation of Airplane General Motion and Control as Inverse Problem," *Journal of Guidance, Control, and Dynamics*, Vol. 9, No. 2, 1986, pp. 198–204.

[21]Asseo, S. J., "Decoupling of a Class of Nonlinear Systems and Applications to an Aircraft Control Problem," *Journal of Aircraft*, Vol. 10, No. 12, 1973, pp. 739–747.

[22]Menon, P. K. A., Badgett, M. E., Walker, R. A., and Duke, E. L., "Nonlinear Flight Test Trajectory Controllers for Aircraft," *Journal of Guidance, Control, and Dynamics*, Vol. 10, No. 1, 1987, pp. 67–72.

[23]Lane, S. H., and Stengel, R. F., "Flight Control Design Using Nonlinear Inverse Dynamics," *Automatica*, Vol. 24, No. 4, 1988, pp. 471–483.

[24]Bugajski, D. J., and Enns, D. F., "Nonlinear Control Law with Application to High Angle of Attack Flight," *Journal of Guidance, Control, and Dynamics*, Vol. 15, No. 3, 1992, pp. 761–767.

[25]Azam, M., and Singh, S. N., "Invertibility and Trajectory Control for Nonlinear Maneuvers of Aircraft," *Journal of Guidance, Control, and Dynamics*, Vol. 17, No. 1, 1994, pp. 192–200.

[26]Snell, S. A., Enns, D. F., and Garrard, W. L., Jr., "Nonlinear Inversion Flight Control for a Supermaneuverable Aircraft," *Journal of Guidance, Control, and Dynamics*, Vol. 15, No. 4, 1992, pp. 976–984.

[27]Georgie, J., and Valasek, J., "Evaluation of Longitudinal Desired Dynamics for Dynamic-Inversion Controlled Generic Reentry Vehicles," *Journal of Guidance, Control, and Dynamics*, Vol. 26, No. 5, 2003, pp. 811–819.

[28]Enns, D., Bugajski, D., Hendrick, R., and Stein, G., "Dynamic Inversion: An Evolving Methodology for Flight Control Design," *International Journal of Control*, Vol. 59, No. 1, 1994, pp. 71–91.

[29]Fan, Y., Lutze, F. H., and Cliff, E. M., "Time-Optimal Lateral Maneuvers of an Aircraft," *Journal of Guidance, Control, and Dynamics*, Vol. 18, No. 5, 1995, pp. 1106–1112.

[30]Sinha, N. K., "Application of Bifurcation Methods to the F-18 HARV Open-Loop Dynamics in Landing Configuration," *Defense Science Journal*, Vol. 52, No. 2, 2002, pp. 103–115.

[31]Ananthkrishnan, N., and Sinha, N. K., "Level Flight Trim and Stability Analysis Using Extended Bifurcation and Continuation Procedure," *Journal of Guidance, Control, and Dynamics*, Vol. 24, No. 6, 2001, pp. 1225–1228.

[32]Lichtsinder, A., Kreindler, E., and Gal-Or, B., "Minimum-Time Maneuvers of Thrust-Vectored Aircraft," *Journal of Guidance, Control, and Dynamics*, Vol. 21, No. 2, 1998, pp. 244–250.

[33]Planeaux, J. B., and McDonnell, R. J., "Thrust Contributions to the Spin Characteristics of a Model Fighter Aircraft," AIAA Paper 1991-2887, Aug. 1991.

[34]Lowenberg, M. H., "Bifurcation Analysis as a Tool for Post-Departure Stability Enhancement," AIAA Paper 1997-3716, Aug. 1997.

[35]Komduur, H. J., and Visser, H. G., "Optimization of Vertical Plane Cobralike Pitch Reversal Maneuvers," *Journal of Guidance, Control, and Dynamics*, Vol. 25, No. 4, 2002, pp. 693–702.

[36]Doedel, E. J., Paffenroth, R. C., Champneys, A. R., Fairgrieve, T. F., Kuznetsov, Y. A., Sandstede, B., and Wang, X., "AUTO2000: Continuation and Bifurcation Software for Ordinary Differential Equations (with HomCont)," California Inst. of Technology, Technical Rept., Pasadena, 2001.

[37]Fremaux, C. M., "Spin Tunnel Investigation of a 1/28-Scale Model of the NASA F-18 High Alpha Research Vehicle (HARV) with and Without Vertical Tails," NASA CR-201687, April 1997.

[38]Durham, "Constrained Control Allocation," *Journal of Guidance, Control, and Dynamics*, Vol. 16, No. 4, 1993, pp. 717–725.

[39]Iliff, K. W., and Wang, K. C., "Flight-Determined Subsonic Longitudinal Stability and Control Derivatives of the F-18 High Angle of Attack Research Vehicle (HARV) with Thrust Vectoring," NASA TP-206539, Dec. 1997.

[40]Iliff, K. W., and Wang, K. C., "Flight-Determined Subsonic Lateral-Directional Stability and Control Derivatives of the Thrust-Vectoring F-18 High Angle of Attack Research Vehicle (HARV), and Comparisons to the Basic F-18 and Predicted Derivatives," NASA TP-206573, Jan. 1999.